Journal of Cluster Science (2026) 37:112
https://doi.org/10.1007/s10876-026-03065-4

ORIGINAL PAPER

Low-Temperature Water-Based *De novo* Synthesis of Composites Based on Nanosized ZIF-8 Polymorph and Embedded *Candida rugosa* Lipase

Noor Fazrieyana Hamidon[1,2,3] · Mohamed Ibrahim Mohamed Tahir[2] · Yazid Yaakob[4] · Muhammad Alif Mohammad Latif[1,5] · Emilia Abdulmalek[1,2] · Mohd Basyaruddin Abdul Rahman[1,2,3]

Received: 26 January 2026 / Accepted: 23 June 2026

Abstract

In this study, *Candida rugosa* lipase (CRL) was embedded within nano-zeolitic imidazolate framework-8, nZIF-8 (1:35), synthesized with a zinc(II) ion to 2-methylimidazole (Zn^{2+}: HmeIM) ratio of 1:35 using a water-based, *de novo* synthesis method at ambient temperature without any modulating agents. The optimization of the embedding process focused on three parameters: the molar ratio of zinc(II) ion to 2-methylimidazole (Zn^{2+}: HmeIM), the concentration of partially purified lipase, and the duration of embedding process. Various physicochemical characterization techniques were employed to confirm and analyze the embedded lipase, including powder X-ray diffraction (PXRD), transmission electron microscopy (TEM), and energy dispersive X-ray (EDX) analysis. Additional characterization methods such as thermogravimetric analysis (TGA), N_2 adsorption-desorption measurements, and Fourier transform infrared spectroscopy (FTIR) were also conducted for comprehensive analysis. The amount of lipase successfully embedded was quantified using the standard Bradford assay, with CRL_3@nZIF-8(1:35) (*Candida rugosa* lipase (3.0 mg) immobilized on nano ZIF-8 synthesized with a Zn^{2+}:HmeIM ratio of 1:35) achieving the highest immobilization of 89% with loading capacity of 17.7 mg/g. To evaluate the functional performance of the immobilized enzyme, a p-nitrophenyl palmitate (*p*-NPPal) hydrolysis assay was performed. The results showed a six-fold increase in enzymatic activity compared to the soluble lipase. These findings highlight the potential of nZIF-8(1:35) as a promising support material for lipase immobilization, functioning as a robust protective nanocomposite and as an enhancer of enzymatic performance, with the added capability of reusability in the CRL_3@nZIF-8(1:35) system.

Keywords Nanosized ZIF-8 · *Candida rugosa* lipase · Embedment into ZIF-8 · Hydrolytic activity

✉ Mohd Basyaruddin Abdul Rahman
basya@upm.edu.my

1 Integrated Chemical BioPhysics Research, Faculty of Science, Universiti Putra Malaysia (UPM), UPM, Serdang, Selangor Darul Ehsan 43400, Malaysia

2 Department of Chemistry, Faculty of Science, Universiti Putra Malaysia (UPM), Serdang, Selangor Darul Ehsan 43400, Malaysia

3 Foundry of Reticular Materials for Sustainability (FORMS), Institute of Nanoscience and Nanotechnology (ION2), Universiti Putra Malaysia (UPM), Serdang, Selangor Darul Ehsan 43400, Malaysia

4 Department of Physics, Faculty of Science, Universiti Putra Malaysia (UPM), Serdang, Selangor Darul Ehsan 43400, Malaysia

5 Centre of Foundation Studies for Agricultural Science, Universiti Putra Malaysia (UPM), Serdang, Selangor Darul Ehsan 43400, Malaysia

Introduction

Candida rugosa lipase (CRL) is a versatile and widely studied biocatalyst, valued for high activity, and convincing substrate specificity. Despite these advantages, the direct use of lipase as a homogeneous catalyst is not economically viable, as it is difficult to recover in its soluble form and may lead to contamination of the final product [1]. Lipase is one of the most widely recognized enzymes in industrial biotechnology, playing a central role in numerous applications [2]. Owing to their remarkable selectivity, lipases are highly versatile catalysts employed in the production of emulsifiers, biodiesel, cosmetics, pharmaceuticals, flavors, fragrances, and various organic compounds [3]. Naturally, lipases differ in their positional specificity, and some lipases can fully hydrolyze triglycerides to glycerol and fatty acids, while others selectively at certain ester bonds. CRL is

Published online: 09 July 2026

widely reported to hydrolyze ester bonds at the sn^1 and sn^3 positions, producing monoglycerides and fatty acids as the main products. However, their broader industrial use faces several challenges, including limited recyclability, susceptibility to denaturation outside physiological environments, and loss of catalytic activity under synthetic conditions, all of which increase operational costs [4].

To overcome these limitations, lipases are often immobilized to facilitate retention, recycling, and improve feasibility at the laboratory scale, enabling subsequent upscaling to industrial applications [5, 6]. Immobilization has been shown to enhance enzyme stability against heat, pH of reaction medium, and other stress conditions, thereby extending their lifespan [7]. Among various immobilization materials, nanomaterials have attracted significant attention due to their high surface area and ability to encapsulate or embed enzymes effectively. Examples include carbon nanotubes, nanofibers, nanocomposites, sol-gel-based nanomaterials, nanorods, and nano-metal organic frameworks (nMOFs) [8, 9].

The thermophilic lipase QLM (from *Alcaligenes* sp.) was successfully embedded within zeolitic imidazolate framework-8 (ZIF-8) using a biomimetic mineralization approach [10]. Characterization analyses confirmed that the lipase was effectively entrapped during ZIF-8 crystal growth. Similarly, cytochrome C (cyt C) was directly incorporated into ZIF-8 via a co-precipitation method, with polyvinylpyrrolidone (PVP) acting as a stabilizer in methanol [3]. These examples demonstrate the potential of ZIF-8 as protective scaffold for enzymes under harsh conditions. Other MOFs, such as ZIF-90 [11], zirconium MOF PCN-128y [12], and IR MOF-74 [13] have also been explored as promising supports for enzyme stabilization. Enzyme immobilization within MOFs typically occurs in larger pores to maintain mobility, but enzymes can also rearrange to fit smaller pores through interactions with functional groups that facilitate immobilization.

Factors such as surface chemistry, solvent choice, and operating conditions strongly influence enzyme positioning and stability. High temperatures often promote enzyme unfolding, whereas lower temperatures help preserve their native structure. Molecular dynamics (MD) simulations of CRL with ZIF-8 revealed the formation of stable complexes supported by strong intermolecular interactions. Residues including Glu-66, Thr-132, Ser-209, Ser-450, and Asn-451 were identified as important for binding, with hydrogen bonding playing an essential role in sustaining catalytic activity [14]. This information provides a molecular-level framework for understanding enzyme-MOF interactions and highlights the potential of lipase-MOF composites in biocatalysis. The MD simulations further support the concept that smaller and restricted pores can protect enzyme activity and enhance reusability.

This research focuses on introducing a *de novo* strategy in which CRL actively directs the crystallization of nano-ZIF-8 at the molar ratio of zinc(II) ion to 2-methylimidazole of 1:35, yielding enzyme-MOF composites with altered structural properties and enhanced catalytic stability. Many studies have reported on the biomimetic mineralization of CRL with ZIF-8 [15, 16]. However, none have addressed the polymorphism of ZIF-8 structures. This work demonstrates the dual role of lipase as both a biocatalyst and a structural modifier of MOF, highlighting its versatility, reusability, and protective effect during the hydrolysis of *p*-nitrophenyl palmitate (*p*-NPPal). Nano-ZIF-8 was selected as the MOF support due to its high surface area, excellent chemical and thermal stability, and well-defined porosity [17–19].

Lipase from *Candida rugosa* was chosen as the model enzyme because of its widespread application in hydrolysis processes and its suitability for various processes, including esterification and transesterification. A *de novo* synthesis approach was employed to grow nano-ZIF-8 crystals around CRL, resulting in highly porous CRL-loaded nano-ZIF-8 composites. The influence of lipase on the crystallization process was investigated, including its effects on crystallinity, particle size, morphology, and porosity of the resulting composites. Since lipase molecules are larger than the pores of nano-ZIF-8, their embedment within the framework adds complexity to understanding the biocatalytic behavior of the embedded system. To evaluate catalytic performance, a comparative hydrolysis study was conducted between embedded CRL and soluble CRL to determine whether the observed differences were due to the protective effect of nano-ZIF-8.

Furthermore, the versatility of the CRL@nano-ZIF-8 system was demonstrated by its application in the hydrolysis of *p*-NPPal, enabling evaluation of the reusability and recovery of the immobilized enzyme. Hydrolysis reactions are commonly employed to evaluate and compare the catalytic activity of immobilized and soluble lipases. In particular, the hydrolysis of *p*-NPPal yields *p*-nitrophenol (*p*-NP) [20]. The amount of *p*-NP released can be quantified spectrophotometrically using UV-Vis analysis [21]. This embedding strategy not only protects enzymes from harsh conditions (such as prolonged time, pH media, and temperature) but also enhances their catalytic activity, making them suitable for nano-biocatalysis applications. Previous findings emphasize the critical role of linker ratio adjustments in determining the structural properties of nano-ZIF-8. Specifically, a higher proportion of linker was essential for achieving nano-ZIF-8 particles [17]. Among the tested ratios, nZIF-8(1:35) exhibited superior characteristics, including high porosity, high surface area, and remarkable

thermal stability, establishing it as an ideal support material for embedding CRL.

The motivation of this work was to demonstrate that such embedment system not only achieves optimal immobilization and loading capacity but also significantly impacts enzymatic activity, stability, and reusability. Overall, this study highlights the advancement of enzyme immobilization technologies for sustainable nano-biocatalytic applications. Previously reported studies showed that immobilizing CRL within ZIF-8 enabled the hydrolysis of *p*-NPPal into *p*-NP, its application in catalysing lactose caprate ester, and revealed its potential in anticancer, demonstrating that immobilized CRL with ZIF-8 can bridge industrial bioprocessing with biomedical applications [15]. This study provides compelling evidence that the embedded system can serve as a foundation for broader applications. Such composites are not only relevant but critically important for advancing future research, opening pathways to diverse application that extend well beyond hydrolysis.

Experimental

Material

Lipase from *Candida rugosa* (CRL), with a specific enzyme activity of 700 U/mg (Enzyme activity, Unit per milligram of protein) meaning that every 1 mg can perform a number of catalytic reactions of 700 units of activity, 2-methylimidazole, and zinc nitrate hexahydrate were obtained from Sigma-Aldrich Ltd. (St. Louis, USA). 4-nitrophenol was purchased from Across-Organic, USA, while 4-nitrophenyl palmitate was supplied by Sigma-Aldrich, Japan. Phosphate buffer solution was purchased from R & M Chemicals (United Kingdom). Additional chemicals with a purity greater than 99%, including acetone and ethanol, were supplied by Qrec Chemicals (New Zealand). Deionized water was prepared using a water purification system, with a resistivity exceeding 18.2 MΩ·cm.

Water-Based Synthesized Nano-ZIF-8

nZIF-8(1:8), nZIF-8(1:21), and nZIF-8(1:35)were synthesized using a modulator-free, water-based method, as previously described by Hamidon et al. (2022, 2023) [17, 18]. The method of synthesizing the material was modified from the previously reported ZIF-8 [22, 23]. The method was modified by eliminating the ageing process and increasing the drying temperature in the evacuation process from 60 °C to 100 °C. In a typical reaction, zinc nitrate hexahydrate solution (1 mmol, 7 mL water) was added to a 2-methylimidazole solution (8 mmol, 15 mL water), forming nZIF-8(1:8). The mixture slowly turned milky after dropwise mixing. The reaction was continuously stirred for 60 min at 150 rpm. The product was collected by centrifugation at 10,000 rpm for 15 min, washed five times with deionized water, and then dried overnight in an oven at 100 °C. The solid sediment was re-dispersed in acetone, a lower-boiling-point solvent, to eliminate the water content before activating the sample overnight in an oven at 100 °C. The product yields of the polymorphisms of ZIF-8 were calculated based on the stoichiometric formula, considering zinc nitrate hexahydrate (g) as the limiting reactant for the reaction [23–25]. According to the stoichiometric equation of a chemical reaction, the limiting reactant is responsible for achieving the complete conversion of the substrate into the final product. The nZIF-8(1:21) and nZIF-8(1:35) were subjected to the same procedure by changing the Zn^{2+}: HmeIM molar ratios to 1:21 and 1:35. All samples had the same reaction time, stirring rate, volume of water, and pre-treatment procedure.

Water-Based Synthesis of Embedded *Candida rugosa* Lipase Onto Nano-ZIF-8

In a typical reaction, a solution of 2-methylimidazole (0.2189 mg/mL, 8 mmol, 15 mL) was added to partially purified lipase (50 mg/mL, 4 mL) to form the HmeIM-CRL solution. Subsequently, a solution of zinc nitrate hexahydrate (0.0992 g/mL, 3mL) was slowly introduced, during which the mixture gradually changed from brown to milky brown. The reaction mixture was stirred continuously at 150 rpm for 60 min. The resulting precipitate was collected by centrifugation at 4 °C and 10,000 rpm for 15 min, followed by washing with deionized water. The samples were then dried overnight in a lyophilizer at temperatures ranging from 50 °C to −80 °C. All samples were prepared under identical conditions, including reaction time, stirring rate, total volume of water, and washing procedure. The Bradford method [26] was used to determine protein content (Fig. S1). The efficiency of the enzyme was calculated as the percentage of immobilization (Eq. 1) based on previously reported formulas [26, 27] and the loading capacity was calculated based on Eq. 2.

$$Immobilization\ (\%) = \frac{Total\ amount\ of\ protein\ (before - after)\ immobilization}{Total\ amount\ of\ protein\ before\ immobilization} \times 100\% \quad (1)$$

$$Loading\ Capacity\ (\%) = \frac{Mass\ of\ lipase\ embedded\ (mg)}{Mass\ of\ nZIF{-}8\ (g)} \quad (2)$$

Commercial *Candida rugosa* lipase was partially purified by dissolving lipase (200 mg) in deionized water (4 mL) with continuous stirring for 30 min in 150 rpm. The mixture

was the centrifuge at 4 °C and 10,000 rpm for 15 min. The supernatant was used as partially purified lipase prior for use.

Physicochemical Characterization

The crystalline phases of the prepared samples were analyzed using powder X-ray diffraction (PXRD) on a Shimadzu XRD-D6000 instrument equipped with CuKα radiation (λ = 1.5418 Å). Scans were performed over a 2θ range of 5°–55° at a scan rate of 2° min^{-1}. Sample morphology was characterized by transmission electron microscopy (TEM) equipped with energy dispersive X-ray (EDX) using a JEM-ARM200F operating at 200 kV. For TEM analysis, the samples were dispersed in ethanol, ultrasonicated for 10 min, and deposited onto a carbon-coated copper grid for imaging. Field emission scanning electron microscopy (FESEM) images were obtained using a JEOL 7600 F. For FESEM, samples were mounted on a carbon-coated copper grid and sputter-coated with a thin layer of gold to prevent charging under the electron beam. Imaging was carried out at an accelerating voltage of 5.0 kV. Nitrogen adsorption-desorption measurements at 77 K were conducted using a TriStar II Plus Series (Micromeritics) to determine surface area and pore characteristics. Prior to analysis, samples were degassed at 120 °C for 8 h to eliminate moisture and residual gases. Surface area and pore volume were evaluated using the Brunauer-Emmett-Teller (BET) and Non-Local Density Functional Theory (NLDFT) models. Thermogravimetric analysis (TGA) was performed using a TGA/SDTA 851 (Mettler Toledo), with samples heated from 50 °C to 800 °C at a rate of 10 °C min^{-1} under an airflow of 1 mL min^{-1}.

Analysis of Protein Gel

Supernatant were collected and concentrated using ultracentrifugation. In this work, a Vivaspin Turbo 15 (30 kDa) and a polyethersulfone (PES) membrane was used to concentrate the supernatant by removing water content after the embedment. The total solution volume was reduced from 45 mL to 4 mL at 60,000 rpm and 4 °C for 6 h. The concentrated supernatant was then analyzed by sodium dodecyl sulfate-polyacrylamide gel electrophoresis (SDS-PAGE), a common laboratory method for separating proteins by molecular weight [28].

Determination of Lipase Activity

The activity of soluble and embedded lipases was assayed spectrophotometrically by measuring the hydrolysis of *p*-nitrophenyl palmitate (*p*-NPPal). The activity of soluble or embedded lipase was measured by adding 1 mg of soluble lipase or 60 mg of embedded lipase to the assay mixture, which consisted of 2 mL of 35.0 mM *p*-NPP in ethanol and 2 mL of PBS at pH 7.4, and incubating under various reaction conditions differing in temperature and pH value. Both soluble and embedded lipases catalyzed the formation of *p*-nitrophenol, which was quantified at 401 nm (Figure S2). One unit of lipase activity (1 U) is defined as production of 1 µmol of *p*-nitrophenol per min under the assay conditions.

Reusability Study of Embedded Lipase in Hydrolysis of *p*-nitrophenyl Palmitate

The hydrolysis activity of the embedded lipase (CRL_3@nZIF-8(1:35)) as a biocatalyst was tested using *p*-NPPal. A clean centrifuge tube was filled with 60 mg of biocatalyst and 2 mL of phosphate-buffered saline (PBS) solution at pH 7.4 to initiate the reaction. Then, 2 mL of 34.0 mM *p*-NPPal in ethanol was added to the mixture and incubated for 15 min at 60 °C before centrifugation for 10 min at 6,000 rpm. The yellow color formed during the hydrolysis process was due to the release of *p*-nitrophenol (*p*-NP) from *p*-NPPal. A UV/VIS spectrophotometer was used to measure the absorbance of released *p*-NP at 401 nm. To determine the lipase activity of the biocatalyst, comparable hydrolysis tests were conducted with nZIF-8(1:35) as a blank. Both CRL_3@nZIF-8(1:35) and nZIF-8(1:35) were washed once with water and then with acetone before reuse. The CRL_3@nZIF-8(1:35) was dried in an oven at 60 °C (below the melting and boiling points of *p*-NP and *p*-NPPal) for 24 h and then further analyzed by PXRD to determine the crystallinity of CRL_3@nZIF-8(1:35) after being recycled up to seven reaction cycles.

Results and Discussions

Characterization and Analysis of Embedded Lipase on nZIF-8

This study builds on our previous findings, which demonstrated that nZIF-8 polymorphism significantly influences its crystallinity, porosity, and particle size [17, 18]. The structural analysis revealed that nZIF-8 with a Zn^{2+}: 2-methylimidazole ratio of 1:8 exhibited diffraction features similar to the simulated ZIF-L pattern, typically associated with micron-sized crystals. In contrast, nZIF-8 prepared with ratios of 1:21 and 1:35 showed diffraction patterns consistent with the ZIF-8 simulated structure, indicating the formation of nanosized particles. This difference highlights how varying precursor ratios favor ZIF-L-like micron structures, while higher ratios promote ZIF-8-like nanoscale frameworks. Here, lipase embedding

was performed using three distinct polymorphic forms of nZIF-8: nZIF-8(1:8), nZIF-8(1:21), and nZIF-8(1:35), corresponding to zinc-to-linker molar ratios of 1:8, 1:21, and 1:35, respectively. Powder X-ray diffraction (XRD) analysis revealed that the crystallinity of the lipase-embedded composites closely resembled that of their respective pristine nZIF-8 polymorphs. However, a noticeable reduction in peak intensity was observed across all polymorphs after lipase embedding (Fig. 1). This attenuation suggests partial structural modification of the nZIF-8 framework due to lipase embedding, resulting from interactions during the embedding process.

Lipase content was quantified using the Bradford assay, with bovine serum albumin (BSA) as the calibration standard [29]. The amount of lipase embedded during the self-assembly process was expressed as immobilization (%) following the method described in previous work [26, 27]. All three ZIF-8 polymorphs (nZIF-8(1:8), nZIF-8(1:21), and nZIF-8(1:35)) successfully embedded *Candida rugosa* lipase (CRL). Among them, nZIF-8(1:35) exhibited the

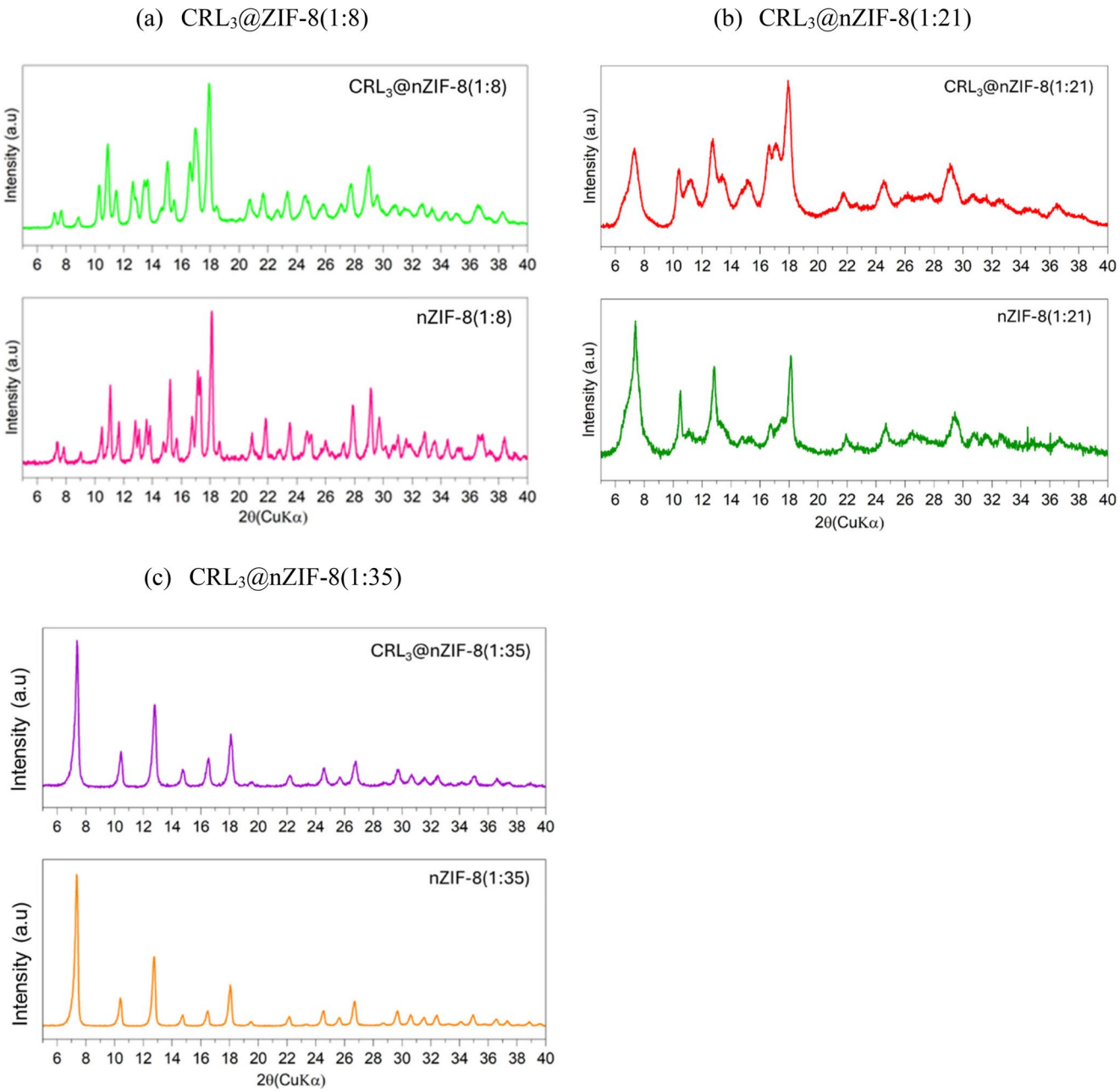

Fig. 1 PXRD pattern of embedded lipase using ZIF-8 polymorphs (**a**) CRL_3@nZIF-8(1:8), lime green (**b**) CRL_3@nZIF-8(1:21), red and (**c**) CRL_3@nZIF-8(1:35), purple with partially purified concentration of 50 mg/mL, molar ratio of Zn^{2+}:HmeIM: Zn, 1:8 (nZIF-8(1:8), pink label), 1:21 (nZIF-8(1:21), green label) and 1:35 (nZIF-8(1:35), orange label) [17]

highest immobilization (89±0.2%), followed by nZIF-8(1:21) (38±0.2%) and nZIF-8(1:8) (24±0.2%) (Fig. 2(a)). The loading capacity of the lipase was calculated based on the absolute amount of lipase embedded within the supports. The values obtained for nZIF(1:8), nZIF-8(1:21) and nZIF-8(1:35) embedded in 50 mg/L of soluble lipase were 4.5±0.01 mg/g, 6.2±0.01 mg/g, and 17.7±0.01 mg/g, respectively. These results demonstrate that CRL_3@nZIF-8(1:35) exhibits the highest immobilization (%) as well as the highest loading capacity (mg/g).

In previous study, CRL was immobilized on chromium terephthalate MIL-101 (MIL-101(Cr)) and three of its chemically modified forms: amino MIL-101(Cr) (NH_2-MIL), trichlorotriazine amino MIL-101(Cr) (TCT@NH_2-MIL) and glutaraldehyde amino MIL-101(Cr) (Glu@NH_2-MIL) [30]. Among these, CRL@Glu@NH_2-MIL exhibited the highest specific activity, with a lipase loading of approximately 55 µg/mg [30]. Both methods relied on pre-synthesized MOFs, followed by immobilization through adsorption or wet impregnation techniques. Comparing this work with previous studies shows that this MOF selection (nZIF-8(1:35)) and method (*de novo*) are more effective, as the loading capacity is higher than that reported on earlier studies. These results highlight the important role of the linker-to-metal ratio in determining the structural properties of nZIF-8, the method use and its compatibility for achieving higher levels of lipase embedding.

Nano-sized ZIF-8 particles, characterized by a higher surface-to-volume ratio, abundant surface sites, faster nucleation, and more efficient confinement of lipase during crystal growth, provide an enhanced environment for enzyme immobilization and catalytic stability. The nZIF-8(1:35) facilitates optimal interactions between lipase molecules and the zinc(II) ions, as well as the 2-methylimidazole linkers, thereby enhancing enzyme immobilization within the framework. This increased accessibility results in approximately 89±0.2% of lipases being embedded. In contrast, micron-sized ZIF-8 particles have a lower surface-to-volume ratio, which limits lipase accessibility and causes steric hindrance. Consequently, the interaction between lipase molecules, zinc and 2-methylimidazole is reduced, yielding only about 24±0.2% lipase embedded. The larger ZIF-8 particle size (nZIF-8 (1:8)) limits lipase embedding during crystal growth, thereby decreasing overall loading efficiency compared to nanosized ZIF-8 (nZIF-8(1:35)).

To further optimize the embedding process, the effect of reaction time on lipase embedding was investigated for nZIF-8(1:35), the nanosized ZIF-8, at intervals of 15, 30, 45, 60, and 75 min (Fig. 2b). The embedded percentage ranged from 16±0.2% to 89±0.2%, with the maximum achieved at 60 min, indicating this as the optimal incubation period. Beyond 60 min, a decline in embedded lipase was observed, suggesting that the self-assembly process had reached equilibrium and that prolonged reaction times may induce lipase leaching due to extended physical agitation. A review of lipase immobilization by physical adsorption highlights that mechanical agitation promotes enzyme desorption due to weak binding forces, limiting reusability in the immobilization process [31]. Other reviews have discussed that, among immobilization methods, adsorption-based immobilization suffers from leaching under strong agitation, and recommend covalent coupling or entrapment to improve stability

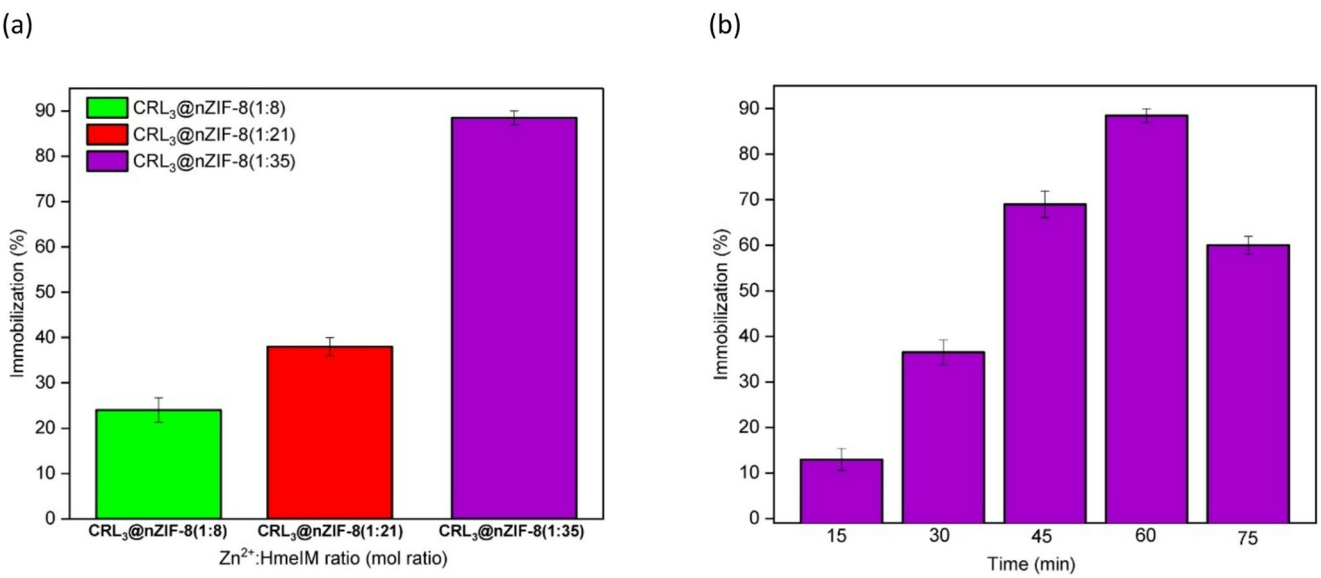

Fig. 2 (**a**) Immobilization (%) of lipase using different ZIF polymorphs at various HmeIM concentrations: 8 (CRL_3@nZIF-8(1:8)), 21 (CRL_3@nZIF-8(1:21)), and 35 (CRL_3@nZIF-8(1:35)); (**b**) Immobilization (%) at various times using nZIF-8(1:35) as the support material, with incubation times ranging from 15 to 75 min

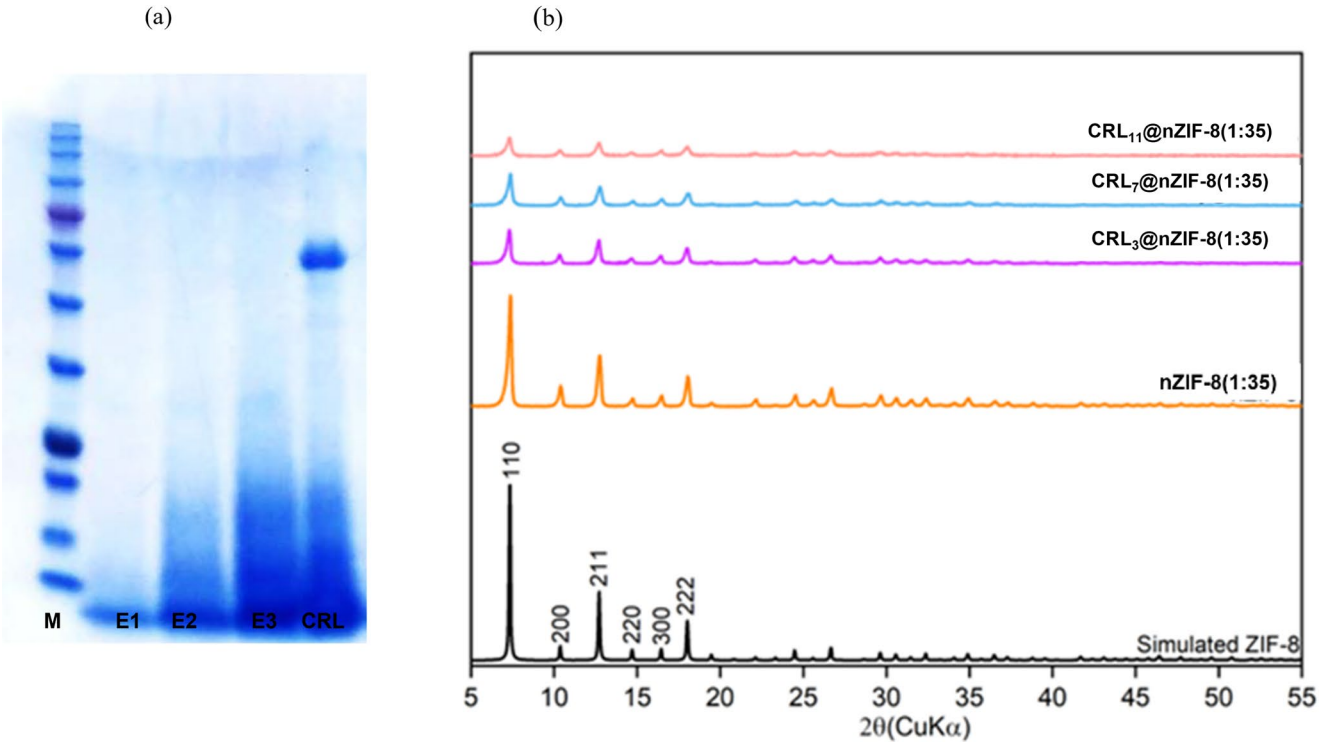

Fig. 3 (**a**) SDS-PAGE gel of supernatant after immobilization (M: Protein marker, E1, E2, E3: CRL_x@nZIF-8(1:35); x = 3,7,11) at different partially purified lipases, (**b**) XRD pattern of CRL_3@nZIF-8(1:35) (purple), CRL_7@nZIF-8(1:35)(blue) and CRL_{11}@nZIF-8(1:35)(pink), referring to the different concentrations of initial enzyme used for the reaction

[32]. Therefore, an incubation time of 60 min is recommended for maximizing lipase embedding within the nZIF-8(1:35) framework. A preliminary screening was conducted to further evaluate the effect of increasing lipase concentration on its embedding efficiency within the nZIF-8(1:35) framework. The concentration of partially purified lipase in the Zn^{2+} and HmeIM (1:35) system was varied from 50 mg/mL to 125 mg/mL and 250 mg/mL. Based on these concentrations, the actual amounts of lipase introduced into the reaction were calculated as 3.0 ± 0.01 mg, 7.0 ± 0.01 mg, and 11.0 ± 0.01 mg for CRL_3@nZIF-8(1:35), CRL_7@nZIF-8(1:35), and CRL_{11}@nZIF-8(1:35), respectively.

It was found that CRL_3@nZIF-8(1:35), CRL_7@nZIF-8(1:35), and CRL_{11}@nZIF-8(1:35) exhibited immobilization percentages of 89%, 90%, and 94%, respectively. The corresponding loading capacities were 17.7, 40.5, and 73.9 mg/g. These results indicate that increasing the concentration of soluble lipase during the embedding process leads to a higher amount of immobilized lipase, as shown by both the immobilization percentage and the loading capacity. To confirm successful embedding, SDS-PAGE analysis was performed on the supernatant solutions obtained after the embedding process. Samples E1, E2, and E3, corresponding to CRL_3@ZIF-8(1:35), CRL_7@nZIF-8(1:35), and CRL_{11}@nZIF-8(1:35), respectively, showed no detectable protein bands (Fig. 3a). This absence of bands suggests that most of the enzyme was successfully embedded within the nZIF-8 structure, leaving negligible amounts in the supernatants. The effect of embedded lipase on the crystallinity of nZIF-8(1:35) was also examined, confirming that the overall crystal structure remained intact after lipase embedding (Fig. 3b). However, a gradual decrease in peak intensity was observed with increasing lipase loading (CRL_3@nZIF-8(1:35) < CRL_7@nZIF-8(1:35) < CRL_{11}@nZIF-8(1:35)). This reduction is likely due to the amorphous nature of *Candida rugosa* lipase, which may partially interfere with the overall crystallinity of the nZIF-8(1:35) framework upon embedding.

The immobilization (%) and loading capacity (mg/g) are summarized in Table 1. The trend shows that nanosized ZIF-8 synthesized at a Zn^{2+}:2-methylimidazole ratio of 1:35 exhibited the highest values. Additionally, increasing

Table 1 Summarizes the calculated capacity loading and immobilization of lipase embedment

Sample	Immobilization (%)	Loading Capacity (mg/g)
CRL_3@nZIF-8(1:8)	24 ± 0.2	4.5 ± 0.01
CRL_3@nZIF-8(1:21)	38 ± 0.2	6.2 ± 0.01
CRL_3@nZIF-8(1:35)	89 ± 0.2	17.7 ± 0.01
CRL_7@nZIF-8(1:35)	90 ± 0.2	45.0 ± 0.01
CRL_{11}@nZIF-8(1:35)	94 ± 0.2	73.9 ± 0.01

the concentration of soluble lipase during the embedding process enhanced both immobilization and loading capacity, with CRL_{11} @nZIF-8(1:35) showing the highest values among the samples.

Physicochemical and Morphological Characterization of Embedded Lipase on nZIF-8(1:35)

The crystallinity of lipase-embedded composites at varying lipase loadings (CRL_x@nZIF-8(1:35), where x = 3, 7, and 11) was analyzed and compared. Relative crystallinity at 2θ = 7°, determined using Gaussian peak fitting, was referenced to pristine nZIF-8(1:35), set as the standard (100% crystallinity). A progressive reduction in crystallinity was observed with increasing lipase content, primarily attributed to the amorphous nature of *Candida rugosa* lipase, which disrupts the ordered framework of nZIF-8(1:35) upon embedding. Specifically, the relative crystallinity decreased from 35% for CRL_3@nZIF-8(1:35), to 33% for CRL_7@nZIF-8(1:35), and further to 21% for CRL_{11}@nZIF-8(1:35), correlating with the incremental enzyme loading. To further evaluate structural changes, crystallite size was calculated using the Scherrer equation, based on peak positions and full width at half maximum (FWHM) values of prominent peaks at 2θ = 7, 10, 12, 14, 16, 18, 22, 24, and 26°. A consistent decrease in crystallite size accompanied the reduction in crystallinity, with values declining from 27 nm (CRL_3@nZIF-8(1:35)) to 22 nm (CRL_7@nZIF-8(1:35)) and 20 nm (CRL_{11}@nZIF-8(1:35)). These findings clearly demonstrate that relative crystallinity and crystallite size in lipase-embedded nZIF-8(1:35) composites are inversely proportional, with both parameters decreasing as lipase loading increases. This inverse relationship is attributed to the amorphous nature of *Candida rugosa* lipase, which introduces structural disorder and broadens the diffraction peak, thereby reducing the range order.

The presence of lipase within nZIF-8(1:35) framework was confirmed using transmission electron microscopy equipped with elemental analysis using Transmission Electron Microscopy and Energy Dispersive X-ray (TEM-EDX) spectroscopy. A comparative study was performed between pristine nZIF-8(1:35) and the lipase-embedded composites (CRL_x@ nZIF-8(1:35) (x = 3, 7, and 11). As shown in Fig. 4, nZIF-8(1:35) exhibited well-defined rhombic dodecahedron morphology [18]. While, the lipase-embedded composites, CRL_x@ nZIF-8(1:35) (x = 3, 7, and 11) displayed noticeable agglomeration of lipase on the particle surfaces, indicating that the relatively large lipase molecules were unable to penetrate the internal pores of ZIF-8 and instead accumulated externally. EDX spectrum of nZIF-8(1:35) (Fig. 4a) displayed characteristic peaks for carbon, nitrogen, zinc, which are typical elements of the ZIF-8 structure. In contrast, the spectra of CRL_2@ nZIF-8(1:35), CRL_7@ nZIF-8(1:35), and CRL_{11}@ nZIF-8(1:35) (Fig. 4b, 4c, and 4d) exhibited additional peaks corresponding to calcium and sulphur. These elements are indicative of *Candida rugosa* lipase, confirming successful lipase embedded within the nZIF-8(1:35) framework during the water-based synthesis process.

Further characterization of CRL_3@nZIF-8(1:35) was performed to study the localization and distribution of lipase within the nZIF-8(1:35)). Five EDX spectra were collected from different regions of the same particle (Fig. 5a). The elemental distribution of N, C, Zn, Ca and S appeared random across these locations, suggesting uneven dispersion of lipase within the nZIF-8(1:35) particles. The content of Ca or S varied between 0.1% and 3.2%, depending on the analyzed region, while Zn, C, and N ranged from 11.5 to 74.2%. Additionally, TEM-EDX line scanning (Fig. 5b) confirmed that lipase was embedded within the ZIF-8, although with a non-uniform distribution. Ca and S were found in CRL_3@ nZIF-8(1:35) which were in accordance with the previously immobilized lipase [33]. These findings validate the successful embedding of lipase within the nZIF-8(1:35) framework and highlight the heterogeneous nature of lipase distribution within the nZIF-8(1:35).

Field Emission Scanning Electron Microscopy (FESEM) images (Fig. 6) provide additional confirmation of successful lipase embedding within nZIF-8(1:35) particles. Comparative analysis of samples before and after washing revealed that lipase was embedded within the internal structure of nZIF-8(1:35) rather than merely adhering to its surface. Notably, the post-washing images showed enhanced clarity and well-defined surface morphology, suggesting that rinsing effectively removed non-embedded, surface-bound lipase. This washing step not only improved visualization of the embedded structures but may also have contributed to enhanced crystallinity by eliminating excess amorphous lipase, which could otherwise interfere with the ordered framework. This is expected to contribute to better catalytic performance by maintaining the integrity of the porous structure and ensuring optimal enzyme confinement.

Fourier Transform Infrared (FTIR) spectroscopy (Fig. 7) was employed to study the functional groups involved in the interaction between *Candida rugosa* lipase (CRL) and the nZIF-8(1:35) framework. The FTIR spectrum of CRL_3@ nZIF-8(1:35) was closely resembled that of pristine nZIF-8(1:35), which aligns with previous reports on enzyme embedment within ZIF-8 [34–36]. This similarity indicates that the enzyme was successfully embedded without causing significant disruption of the host framework's structural integrity. The characteristic bands of nZIF-8(1:35) highlight the interaction between 2-methylimidazole (HmeIM) and Zn^{2+} ions, which form the sodalite (sod) topology. A

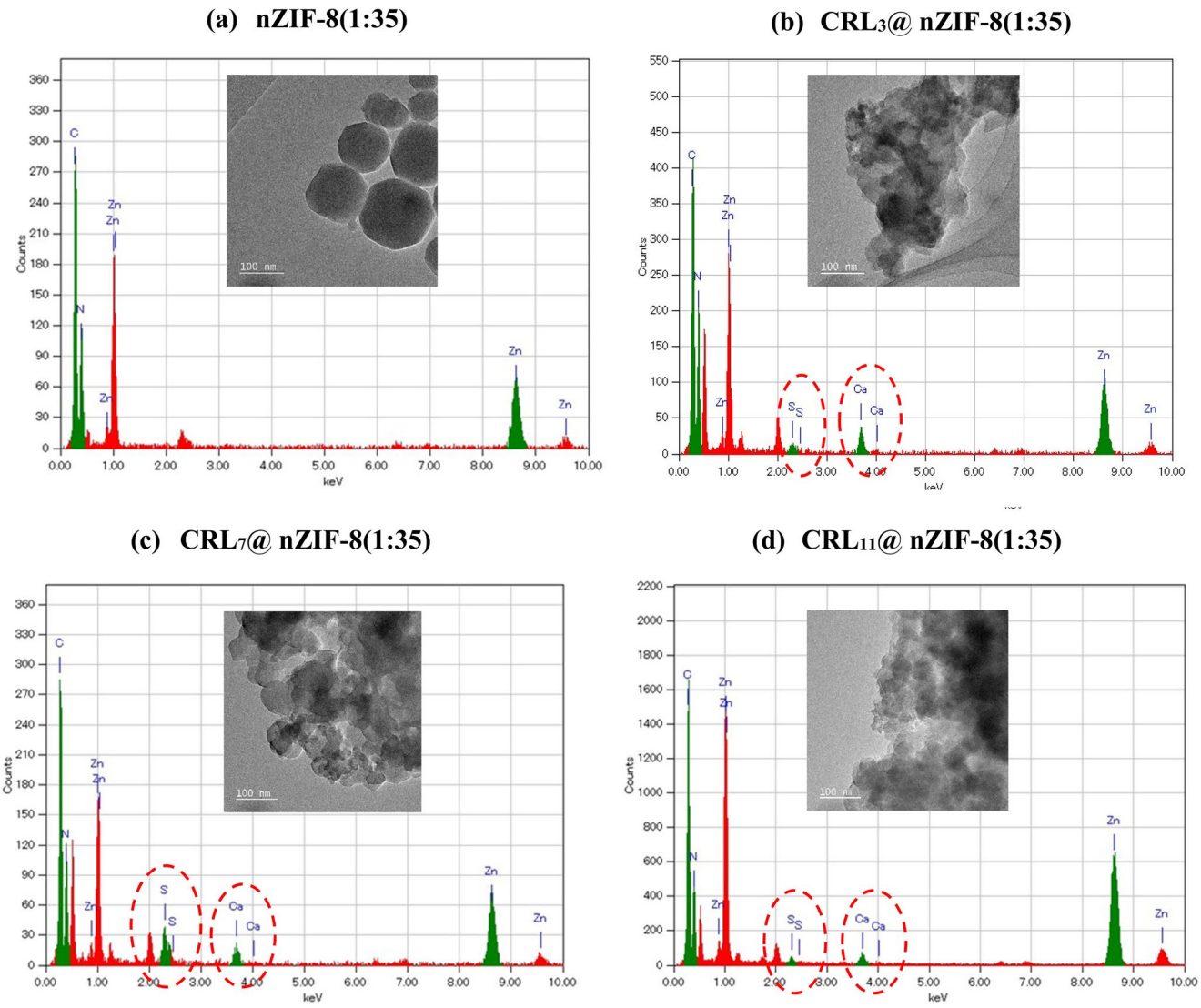

Fig. 4 Energy dispersive X-ray (EDX) spectroscopy of (**a**) nZIF-8(1:35), (**b**) CRL_2@ nZIF-8(1:35), (**c**) CRL_7@ nZIF-8(1:35), and (**d**) CRL_{11}@ nZIF-8(1:35), corresponding to different concentrations of partially purified lipase used for embedded

prominent absorption band at 419 cm^{-1} corresponds to Zn-N bond vibrations, confirming successful coordination between Zn and N atoms in the imidazolate linker. Additional bands in the region 755–1419 cm^{-1} are attributed to the strong bending vibrations of the HmeIM ring, while weak bands observed between 2926 and 3199 cm^{-1} originate from aliphatic and aromatic C-H stretching vibrations of HmeIM. Notably, the spectrum of CRL_3@nZIF-8(1:35) exhibited a distinct band at 1656 cm^{-1}, assigned to the amide I band of the lipase, which corresponds to C=O stretching vibrations. This feature confirms the presence of lipase protein within the nZIF-8(1:35) framework. Furthermore, a noticeable shift in the broad band around 3500 cm^{-1}, associated with N-H stretching, suggests the presence of amino groups from the embedded lipase, providing additional evidence of successful enzyme embedding within nZIF-8(1:35) cage.

The thermogravimetric and differential thermal analysis (TGA-DTA) curves (Fig. 8) illustrate the thermal decomposition behavior of pristine nZIF-8(1:35) and lipase-embedded CRL_3@nZIF-8(1:35) under an air atmosphere at temperatures ranging from 55 to 800 °C. During this process, the organic linker (HmeIM) and the lipase enzyme undergo combustion, while Zn^{2+} is oxidized to zinc oxide (ZnO), which remains as the final residue. For CRL_3@ nZIF-8(1:35), two distinct decomposition events were observed. The first, at approximately 178 °C, corresponds to the thermal degradation of the embedded lipase. The second, near 413 °C, is attributed to the decomposition of the nZIF-8(1:35) framework itself, which functions as a protective embedment. These thermal transitions confirm successful enzyme embedding and provide insight into the thermal stability of the composite system.

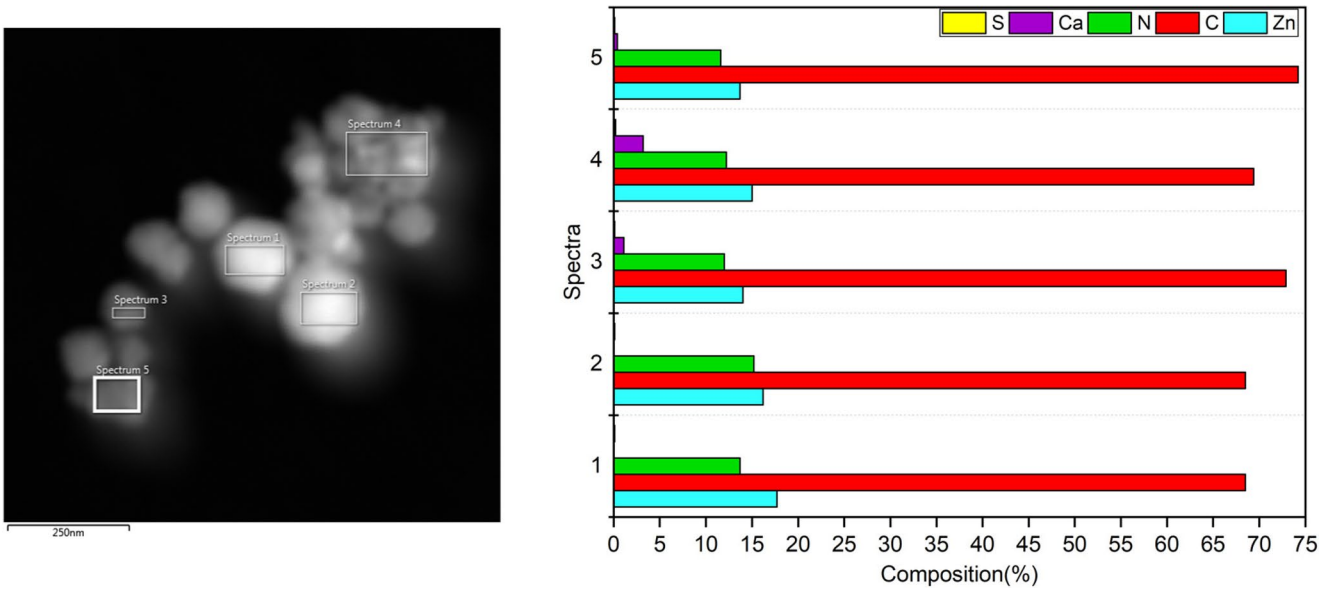

Fig. 5 (**a**) Five different spots and (**b**) the elemental composition of CRL_3@nZIF-8(1:35) by X-ray EDX mapping of each spot

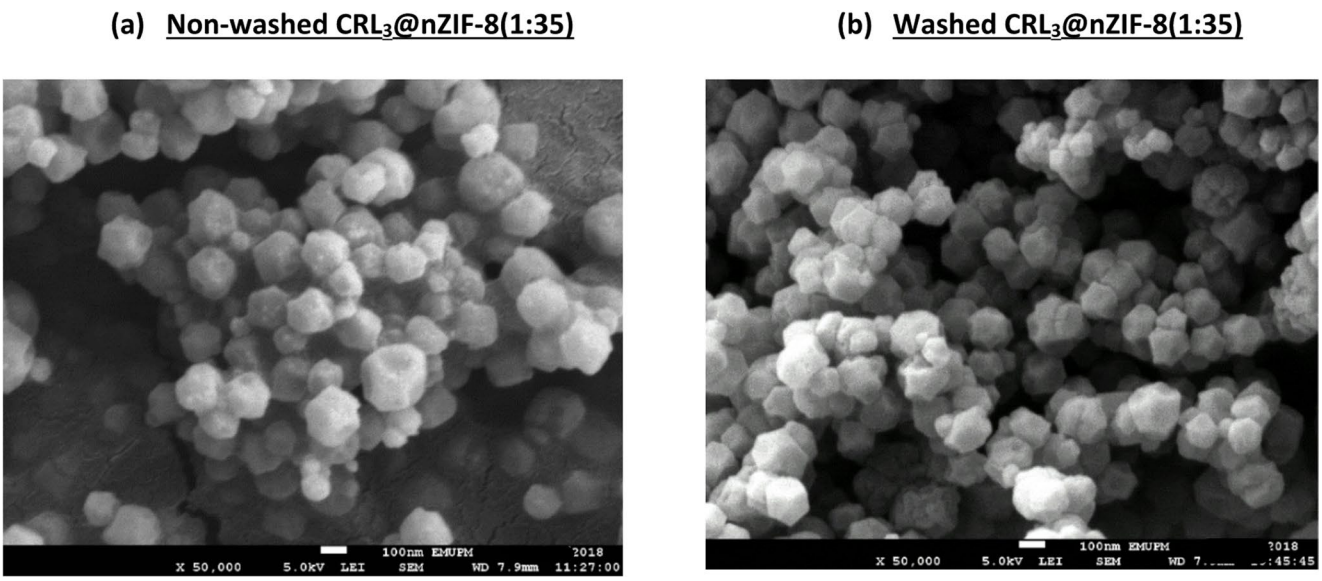

Fig. 6 FESEM images reveal the single-phase morphology of embedded lipase (CRL_3@nZIF-8(1:35)) for (**a**) non-washed and (**b**) washed (right) samples at a magnification of 50,000X

Quantitatively, CRL_3@nZIF-8(1:35) exhibited a gradual and continuous weight loss between 55 and 187 °C, with an overall mass loss of approximately 18%, associated with the decomposition of lipase and removal of adsorbed moisture. In contrast, pristine nZIF-8(1:35) displayed a major decomposition event at around 350 °C, with a total weight loss of 55%. The residual mass was approximately 27%, consistent with ZnO formation. These findings indicate that nZIF-8(1:35) maintains excellent thermal stability under oxidative conditions and can effectively serve as a heat-resistant carrier for lipase, preserving structural integrity up to 413 °C. The TGA results were consistent with previously reported data on immobilized lipase with ZIF-90. The structural integrity of ZIF was retained up to 350 °C [28].

Nitrogen adsorption-desorption analysis (Fig. 9) was performed to evaluate the effect of lipase embedding on the porosity of the nZIF-8(1:35) framework. The Brunauer-Emmett-Teller (BET) method revealed that pristine nZIF-8(1:35) exhibited a surface area of 1776 m^2g^{-1}, indicative of its well-developed porous structure. However, upon lipase embedding, the surface area of CRL_3@nZIF-8(1:35) decreased significantly to 645 m^2g^{-1}, representing a reduction of more than 60%. Similarly, the total pore volume decreased from 0.64 cm^3g^{-1} in pristine nZIF-8(1:35) to

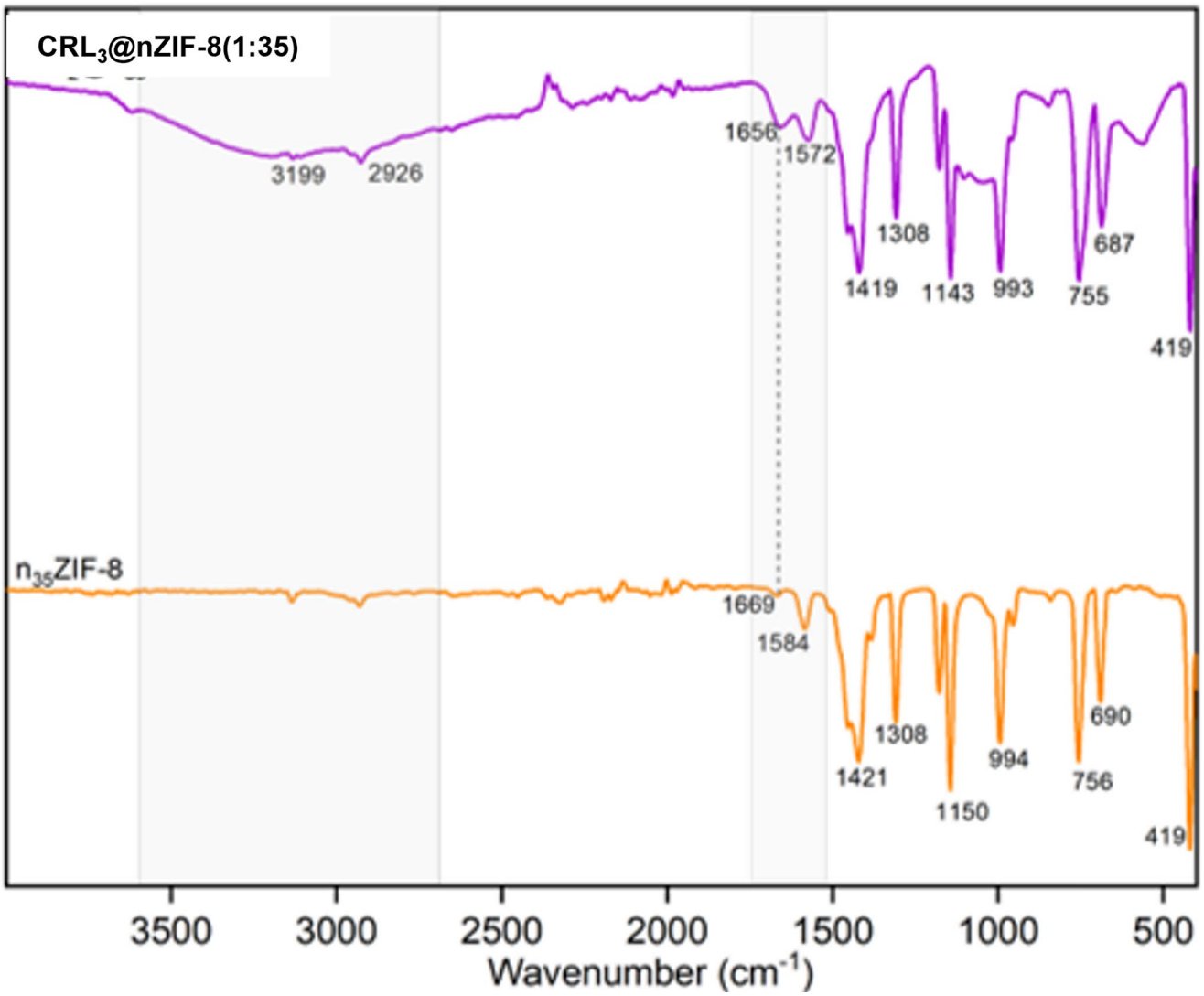

Fig. 7 IR spectra of nZIF-8(1:35) (orange) and CRL_3@nZIF-8(1:35) (purple)

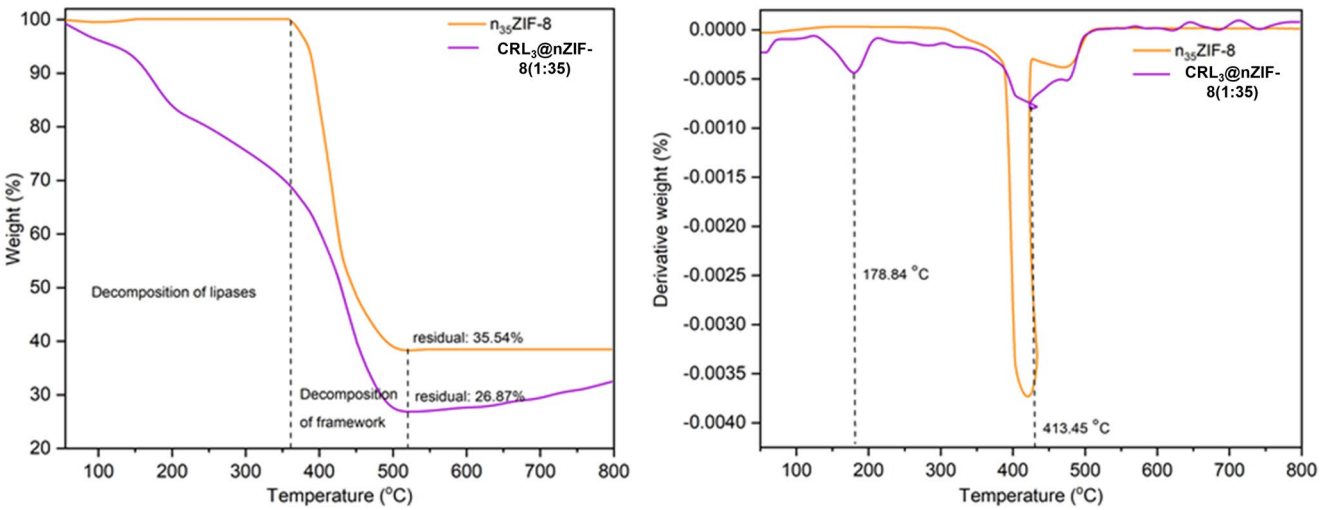

Fig. 8 TGA-DTA trace of nZIF-8(1:35) (orange) and CRL_3@nZIF-8(1:35) (purple), TGA (a), DTA (b) under air in the temperature range of 55–800 °C

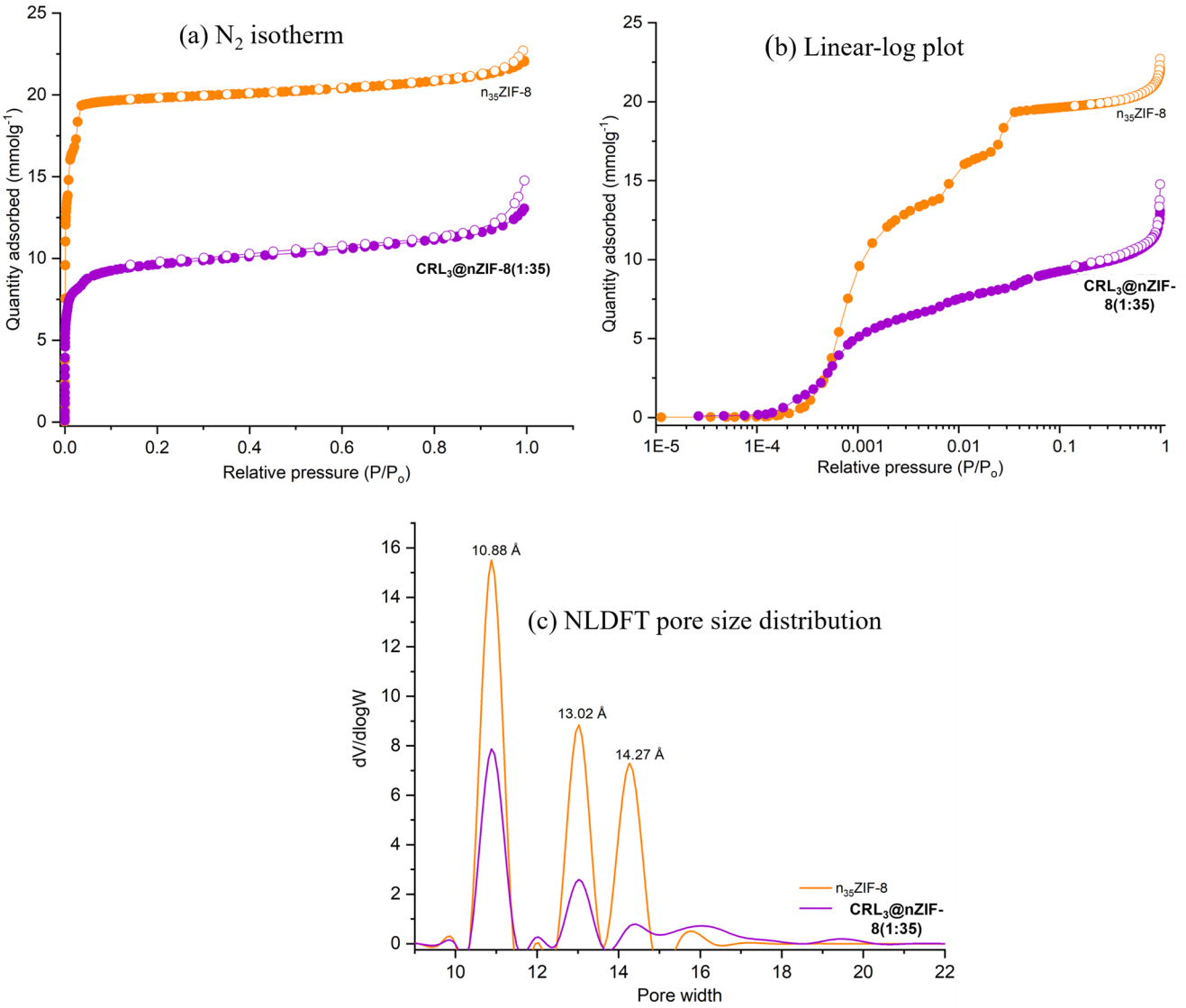

Fig. 9 (**a**) N_2 isotherm, (**b**) linear-log plot, and (**c**) NLDFT pore size distribution, at 77 K. Adsorption and desorption are represented for nZIF-8(1:35) and CRL_3@nZIF-8(1:35)

0.31 cm^3g^{-1} in CRL_3@nZIF-8(1:35), reflecting partial pore blockage caused by the presence of lipase molecules. At low relative pressure (P/Po < 0.06), a sharp decrease in nitrogen adsorption was observed, suggesting that microporosity remains a dominant feature in both materials. A noticeable hysteresis loop appeared near a relative pressure of 1 in CRL_3@nZIF-8(1:35), likely due to the complex interaction between the nZIF-8(1:35) framework and the embedded lipase, which may alter the pore space and influence gas diffusion dynamics. These results confirm successful lipase embedding within nZIF-8(1:35) and demonstrate its impact on the material's textural properties.

The pore characteristics of nZIF-8(1:35) were significantly altered upon lipase embedding, with both surface area and pore volume reduced by more than half. This substantial decrease confirms successfully incorporation of lipase within the framework. The embedding process was achieved by synthesizing nZIF-8(1:35) in the presence of lipases, allowing the framework to grow and the lipases to be embedded during the growth process. Lipase molecules were confined within the void spaces between growing nZIF-8(1:35) crystals during synthesis, effectively embedding them within the framework without compromising overall structural integrity. The optimal enzyme loading selected for this study was CRL_3@nZIF-8(1:35), which achieved an immobilization efficiency of 89%. This corresponds to the embedding of approximately 45 mg/mL of lipase from an initial concentration of 50 mg/mL introduced into the composite system during the embedding process, equivalent to17.7 mg/g of loading capacity. The calculation

showed that in the CRL_3@nZIF-8(1:35) composite, 1 mg of soluble lipase was successfully embedded within 60 mg of the composite material, corresponding to a distribution of 1 mg lipase per 60 mg of composite. To further confirm the lipase activity after the embedding process, hydrolysis of *p*-nitrophenyl palmitate (*p*-NPPal) was tested to determine the activity of the embedded lipase by selecting different parameters for optimization.

Catalytic Activity of CRL_3@nZIF-8(1:35)

When comparing the activity of all embedded samples (CRL_3@nZIF-8(1:8), CRL_3@nZIF-8(1:21), CRL_3@nZIF-8(1:35)) (data not included), CRL_3@nZIF-8(1:35) exhibited the highest catalytic performance, with activity enhanced three- to four-fold compared to the other embedded lipases. This result aligns with the immobilization (%) and loading capacity (mg/g) summarized in Table 1, as previously mentioned in Section 3.2. When comparing CRL_3@nZIF-8(1:35) with CRL_7@nZIF-8(1:35) and CRL_{11}@nZIF-8(1:35) (data not included), CRL_3@nZIF-8(1:35) demonstrated superior catalytic performance, despite a lower loading amount, with activity a fold higher than the other embedded lipases. Several factors contributed to this outcome. First, higher loading may cause partial crowding or aggregation of lipase, restricting substrate diffusion and reducing the effective rate. Second, excessive lipase loading may disrupt the framework, whereas CRL_3@nZIF-8(1:35) maintains an optimal balance between immobilization, loading capacity, and catalytic accessibility.

Therefore, a direct comparison between soluble lipase and CRL_3@nZIF-8(1:35) was conducted, evaluating the activity of the embedded form relative to soluble lipase at various time points (Fig. 10(a)). The relative activity (%) was calculated by normalizing each measurement against the highest lipase activity observed in the dataset. The results showed that at 40 °C, the activity of soluble lipase was lower than that of the embedded form. The optimal reaction time for soluble lipase (100%) was typically within 5 min. Prolonged heat exposure negatively affected soluble lipase activity, causing denaturation and a rapid decline in activity, reaching a minimum of 1% after 75 min. In contrast, the embedded form exhibited optimal activity (100%) within 15 min, indicating that nZIF-8(1:35) acts as a heat-resistant matrix, protecting the active site and maintaining lipase activity for a longer period.

The thermal stability of CRL_3@nZIF-8(1:35) was further assessed in a hydrolysis reaction at a fixed incubation time of 15 min across temperatures ranging from 30 to 99 °C. Typically, catalytic activity increases with temperature, but there is a significant decrease once optimal conditions are exceeded. This decline is due to alterations in the enzyme's active site, leading to gradual denaturation until the enzyme is fully inactivated. The thermal stability of soluble lipase was observed between 30 and 40 °C. Exposure to temperatures above this range negatively affected soluble lipase activity due to heat-induced denaturation and structural changes. As temperature increased, further structural changes led to decreased activity until complete denaturation occurred. Figure 10(b) shows that soluble lipase exhibited its highest activity (100%) at 40 °C, with activity decreasing as temperature increased, reaching only 9% at 70 °C, indicating near-complete denaturation. The activity of embedded lipase was found to be four-folds higher than that of the soluble form. The highest activity of the embedded lipase was 100% at 60 °C. Activity slightly decreased as the temperature increased from 60 to 100 °C. This may be due to temperature changes having only a minor impact on lipase in the embedded form. However, the overall activity of embedded lipase remained above 80%, even at the highest temperature applied. A previous study investigated and compared the activity of soluble and encapsulated CRL in hydrolysis of *p*-NPPal. The optimal temperature for both soluble CRL and encapsulated CRL is 35 °C, at which both exhibit 100% relative activity. When the temperature is further increased to 55 °C, soluble CRL retains only 31% of its activity, whereas encapsulated CRL retains 62% [15]. This work and earlier studies confirm that immobilization strategies not only shift the optimal operating temperature upward but also mitigate thermal deactivation, thereby broadening the applicability of lipases in biocatalysis under harsh conditions.

CRL_3@nZIF-8(1:35) was then tested in a reaction system with different pH media. The pH of the medium ranged from 1 to 13, with acidic, neutral, and basic conditions tested as harsh operational environments. The pH of the medium is also important because nZIF-8(1:35) frameworks can undergo cleavage of Zn–N bonds in very acidic environments, leaving only the zinc(II) cation and the HmeIM anion in the system. The activity of lipase (Fig. 10(c)) decreases beyond the optimal pH due to modifications in the enzyme structure caused by interactions with H^+ and OH^- in the surrounding conditions. However, the embedded lipase demonstrated enhanced activity due to the presence of nZIF-8(1:35) as a protective matrix, shielding the lipase from direct denaturation and preventing a rapid decrease in activity. This improvement is most noticeable at optimal neutral pH values. Both soluble and embedded lipase exhibited optimal activity (100%) at pH 7.4 (the dotted line was redundant), with nZIF-8(1:35) as a protective matrix enabling the embedded lipase to achieve approximately five-fold higher activity compared to the soluble form. Moreover, the embedded lipase consistently demonstrated enhanced performance under extreme

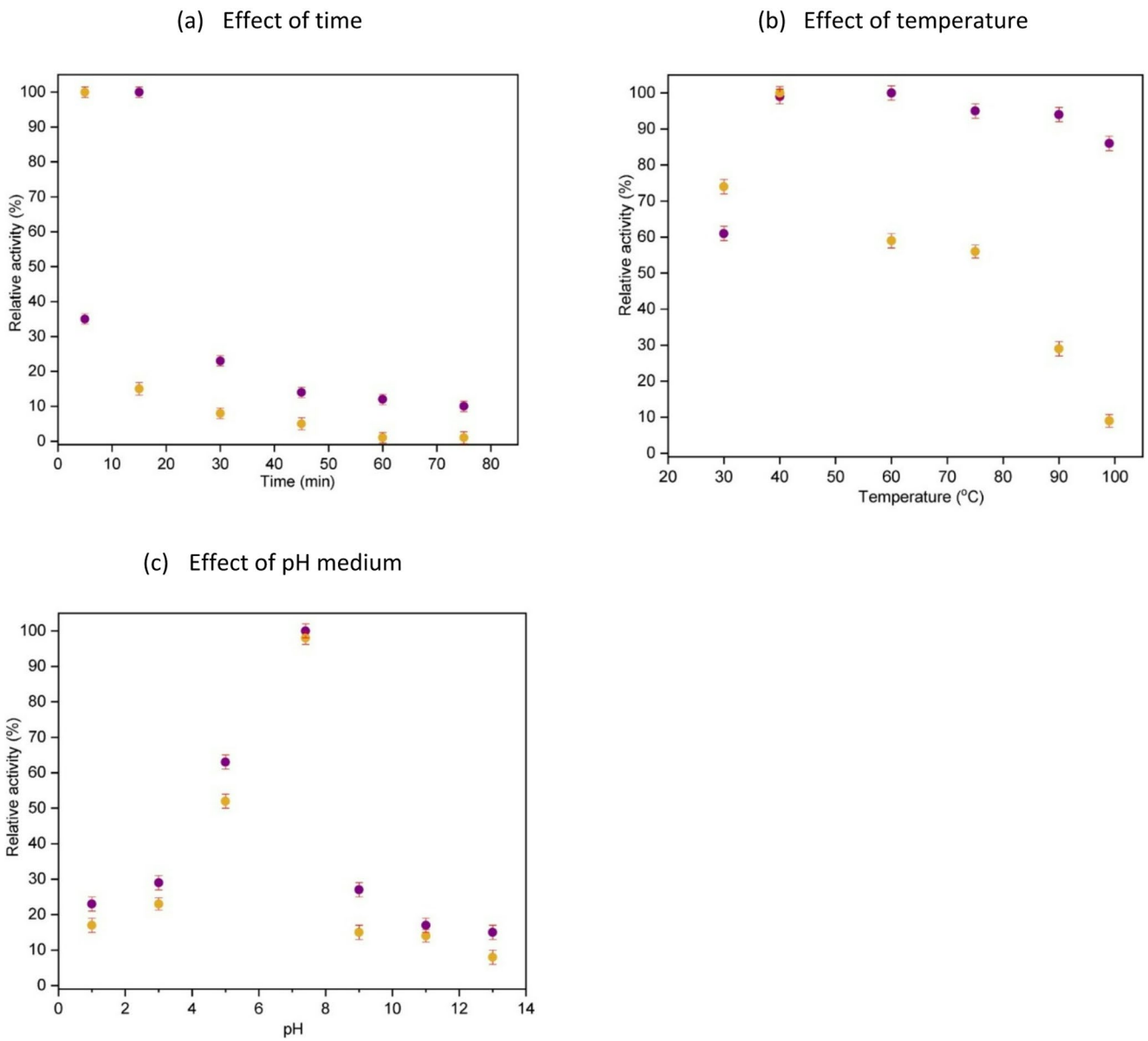

Fig. 10 (**a**): Activity performance of CRL_3@nZIF-8(1:35) and soluble lipase (CRL) at 40 °C over different incubation times (5, 15, 30, 45, 60, and 75 min). (**b**): Activity of CRL_3@nZIF-8(1:35) and soluble lipase (CRL) at different temperatures (30, 40, 60, 75, 90, and 99 °C) with an incubation time of 15 min. (**c**): Activity of CRL_3@nZIF-8(1:35) and soluble lipase (CRL) at different pH values (pH 1, 3, 5, 7.4, 9, 11, and 13) after incubation for 15 min at 60 °C. The yellow dot represents soluble lipase activity, while the purple dot represents embedded lipase activity. Conditions: 2 mL of 35.0 mM *p*-NPPal in ethanol, 2 mL PBS at different incubation times (5, 15, 30, 45, 60, and 75 min), temperatures (30, 40, 60, 75, 90, and 99 °C), or pH values (pH 1, 3, 5, 7.4, 9, 11, and 13), incubated at 90 °C for 15 min. Equivalent amounts of protein or enzyme in soluble and embedded lipase were calculated for 1 mg

pH conditions, whether highly acidic or highly basic. For example, at pH 1, the activity of the embedded lipase was 25%, while that of the soluble lipase was only 17%. This is because soluble lipase is directly affected by pH fluctuations, which can alter its conformation and reduce catalytic efficiency toward *p*-NPPal. In contrast, the presence of nZIF-8(1:35) provides structural protection and stabilization, shielding lipase from denaturation and enabling sustained catalytic activity even under harsh operational conditions. A previously reported study revealed that the maximum observed activity was defined as 100% for comparison between free CRL and encapsulated CRL within the pH range of 6–7. Notably, CRL@ZIF-8 exhibited higher activity than free CRL in both acidic (pH 2–6) and alkaline (pH 7–9) regions, confirming the positive effect of enzyme encapsulation on its performance [15]. These findings significantly improves both thermal stability and pH tolerance of immobilized CRL, thereby extending the

functional applicability of lipases in different biocatalytic processes.

The embedded lipase (CRL_3@nZIF-8(1:35)) demonstrated enhanced catalytic activity, thermal stability, and pH tolerance compared to soluble lipase. The optimized immobilization balances and enhances catalytic accessibility while preventing denaturation under harsh conditions. CRL_3@nZIF-8(1:35) effectively protected lipase, maintaining high activity during prolonged incubation, elevated temperatures, and extreme pH environments.

Reusability Study of Embedded Lipase, CRL_3@nZIF-8(1:35)

Under optimum conditions (CRL_3@nZIF-8(1:35), 15 min of incubation at 60 °C, and a fixed concentration of *p*-NPPal at 35 mM), the reusability of the embedded lipase was evaluated in a hydrolysis reaction. CRL_3@nZIF-8(1:35) was recovered by decanting, washed once with water and then with acetone, and dried in an oven at 100 °C before reuse in the next cycle. The observed yellowing of the embedded lipase suggests that *p*-NP may have been partially trapped within the frameworks, likely contributing to a modest decline in activity in each cycle. Lipase activity gradually decreased over successive cycles (Fig. 11), with a reduction of approximately 10–20% per cycle. After the seventh cycle of *p*-NPPal hydrolysis using recycled CRL_3@nZIF-8(1:35), approximately 20% of the initial lipase activity was retained, demonstrating partial but sustained catalytic performance under repeated use. In each cycle, the recovery rate may play an important role because it reflects the stability of the embedded enzyme and the efficiency of the recovery process. During repeated hydrolysis, the enzyme is subjected to stress factors under optimum conditions that gradually reduce its catalytic activity. By monitoring activity over cycles, CRL_3@nZIF-8(1:35) protects the lipase and is effective in preserving enzyme activity.

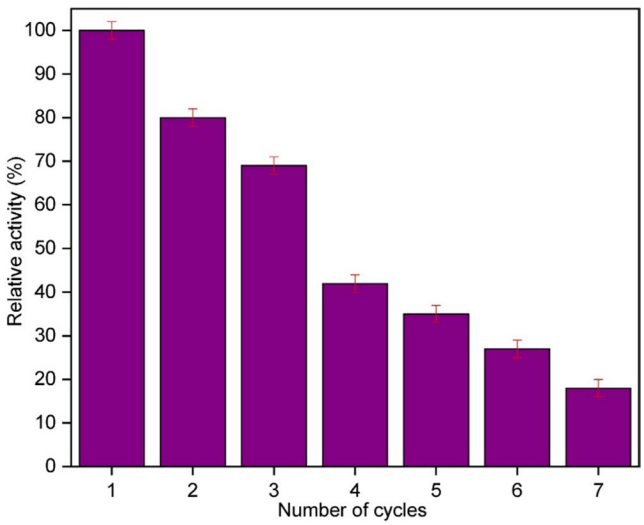

Fig. 11 Reusability study of CRL_3@nZIF-8(1:35) under optimal conditions. Conditions: 2 mL of 35.0 mM *p*-NPPal in ethanol, 2 mL PBS pH 7.4, incubated at 60 °C for 15 min. Equivalent amounts of protein or enzyme in soluble lipase and embedded lipase were calculated for 1 mg

In previous study, FITC-lipase@PCN-333 demonstrated recyclability, retaining up to 77.8% of its relative activity over six cycles, with a 22.4% reduction in enzymatic activity observed in the sixth cycle [37]. Both PCN-333 and ZIF-8 can serve as effective supports for recyclability studies, as soluble lipase cannot be reused directly and requires purification to avoid contamination. PCN-333, with its mesoporous structure, offers a larger pore aperture in the range of 4.2–5.5 nm, making it suitable for accommodating biomolecules such as enzymes. In contrast, ZIF-8 possesses a microporous framework with a much smaller pore aperture of approximately 0.34 nm, which limits direct enzyme embedment but provides strong structural stability and protective embedment.

The PXRD patterns of CRL_3@nZIF-8(1:35) at cycle 1 and cycle 7 (Fig. 12) were compared, and the results demonstrated that each diffraction peak decreased in intensity, indicating partial structural disruption during repeated catalytic cycles. However, the overall crystallinity was maintained, demonstrating strong structural stability and protective embedment provided by nZIF-8(1:35). In addition, these crystalline phases may also be influenced by *p*-NP interacting with the framework during lipase catalysis, leaving residual *p*-NP adsorbed on the surface of the embedded lipase. This interaction could contribute to minor variations in peak intensity while still preserving the fundamental crystalline framework.

Conclusion

In summary, the high-loading embedded lipase was successfully prepared using a *de novo* approach and demonstrated high hydrolytic activity, withstanding several parameters after embedment. Embedment was confirmed by PXRD, which showed a reduction in the intensity of the ZIF-8 polymorph peaks. EDX confirmed the presence of sulfur from the lipase and calcium as a metal ion detected in the elemental analysis. *Candida rugosa* lipase molecules, which are larger than the pore apertures of nZIF-8(1:35), were embedded within the framework during self-assembly rather than adsorbed on the surface. The reduction in pore volume and surface area of CRL_3@nZIF-8(1:35) demonstrates that lipase molecules occupy

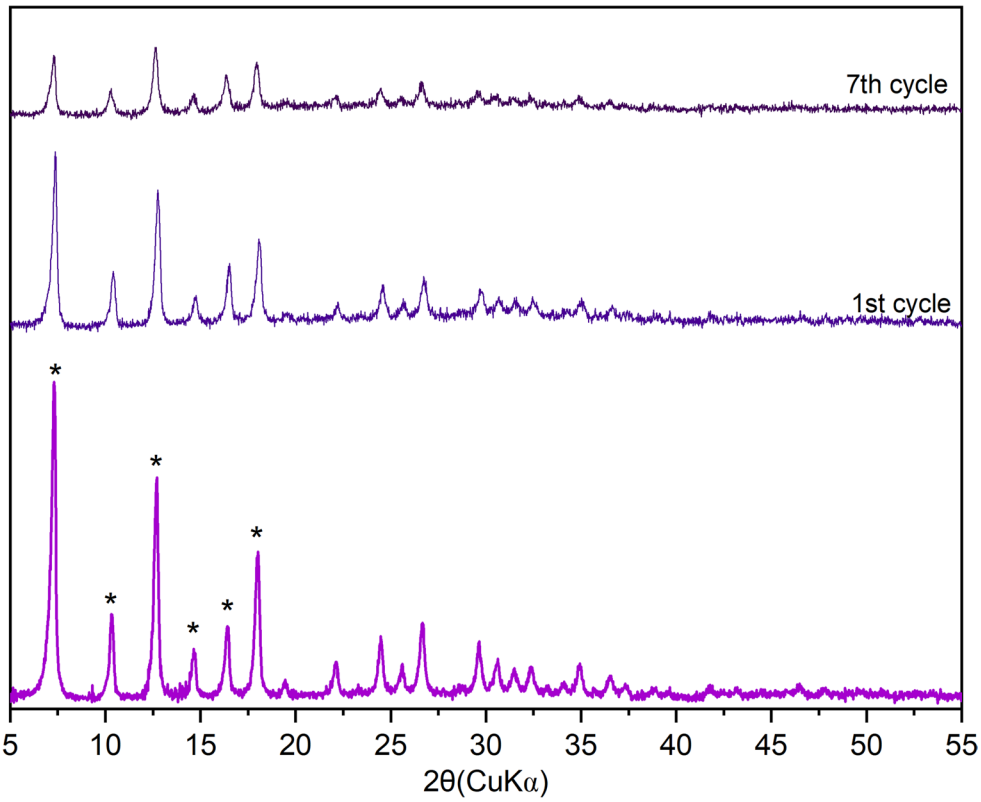

Fig. 12 PXRD pattern of CRL_3@nZIF-8(1:35) after recycling study

and fill the internal voids of the crystals. This embedment enhances catalytic performance, with CRL_3@nZIF-8(1:35) exhibiting six-fold higher activity compared to soluble lipase under the studied conditions. The reusability assessment demonstrated that CRL_3@nZIF-8(1:35) can be applied in repeated hydrolysis reactions, by maintaining the structural integrity of the nZIF-8(1:35) framework for up to seven cycles.

Supplementary Information The online version contains supplementary material available at https://doi.org/10.1007/s10876-026-03065-4.

Acknowledgements This project is supported by Universiti Putra Malaysia (GPB/2017/9570200 and GPI/2023/9777100). Part of this research was conducted at Universiti Putra Malaysia and Nagoya Institute Technology. N.F.H gratefully acknowledge Universiti Putra Malaysia and Ministry of Higher Education Malaysia for the award of fellowship for the study. M.B. A. R. and N.F.H thank Kyle E. Cordova, Dr Ha Lac Nguyen and Professor Omar M. Yaghi for valuable discussion.

Author Contributions N.F.H and M.B.A.R developed the idea. N.F.H performed the material synthesis and biocatalysis synthesis. N.F.H, M.I.M.T, M.B.A.R, M.A.M.L, and K.E.C helped in improving the conceptual design, co-wrote the manuscript and further discussed the characterization part. Y.Y helped further in TEM characterization.

Funding Open access funding provided by The Ministry of Higher Education Malaysia and Universiti Putra Malaysia

Data Availability Data will be made available on request.

Declarations

Competing interests The authors declare no competing interests.

References

1. E. Vanleeuw *et al.*, "Substrate-Specificity of *Candida rugosa* Lipase and Its Industrial Application," *ACS Sustainable Chem. Eng.*, vol. 7, no. 19, pp. 15828–15844, Oct. 2019, doi: https://doi.org/10.1021/acssuschemeng.9b03257.
2. Z. Cabrera, G. Fernandez-Lorente, R. Fernandez-Lafuente, J. M. Palomo, and J. M. Guisan, "Novozym 435 displays very different selectivity compared to lipase from *Candida antarctica* B adsorbed on other hydrophobic supports," *Journal of Molecular Catalysis B: Enzymatic*, vol. 57, no. 1–4, pp. 171–176, May 2009, doi: https://doi.org/10.1016/j.molcatb.2008.08.012.

3. F. Lyu, Y. Zhang, R. N. Zare, J. Ge, and Z. Liu, "One-Pot Synthesis of Protein-Embedded Metal–Organic Frameworks with Enhanced Biological Activities," *Nano Letters*, 2014, doi: https://doi.org/10.1021/nl5026419.
4. X. Wu, J. Ge, C. Yang, M. Hou, and Z. Liu, "Facile synthesis of multiple enzyme-containing metal–organic frameworks in a biomolecule-friendly environment," *Chem. Commun.*, vol. 51, no. 69, pp. 13408–13411, 2015, doi: https://doi.org/10.1039/C5CC05136C.
5. N. N. Ramlee *et al.*, "Biochemical and Physical Characterization of Immobilized *Candida rugosa* Lipase on Metal Oxide Hybrid Support," *Catalysts*, vol. 12, no. 8, p. 854, Aug. 2022, doi: https://doi.org/10.3390/catal12080854.
6. S. Chen, M. Ma, J. Peng, X. He, Q. Wang, and G. Chu, "Rapid prediction method of ZIF-8 immobilized *Candida rugosa* lipase activity by near-infrared spectroscopy," *Spectrochimica Acta Part A: Molecular and Biomolecular Spectroscopy*, vol. 302, p. 123072, Dec. 2023, doi: https://doi.org/10.1016/j.saa.2023.123072.
7. N. R. Mohamad, N. H. C. Marzuki, N. A. Buang, F. Huyop, and R. A. Wahab, "An overview of technologies for immobilization of enzymes and surface analysis techniques for immobilized enzymes," *Biotechnology and Biotechnological Equipment*, vol. 29, no. 2, pp. 205–220, 2015, doi: https://doi.org/10.1080/13102818.2015.1008192.
8. R. A. Meryam Sardar, "Enzyme Immobilization: An Overview on Nanoparticles as Immobilization Matrix," *Biochem Anal Biochem*, vol. 04, no. 02, 2015, doi: https://doi.org/10.4172/2161-1009.1000178.
9. M. R. Mehrasbi, J. Mohammadi, M. Peyda, and M. Mohammadi, "Covalent immobilization of *Candida antarctica lipase* on core-shell magnetic nanoparticles for production of biodiesel from waste cooking oil," *Renewable Energy*, vol. 101, pp. 593–602, Feb. 2017, doi: https://doi.org/10.1016/j.renene.2016.09.022.
10. H. He *et al.*, "Construction of Thermophilic Lipase-Embedded Metal-Organic Frameworks via Biomimetic Mineralization: A Biocatalyst for Ester Hydrolysis and Kinetic Resolution," *ACS Applied Materials and Interfaces*, vol. 8, no. 37, pp. 24517–24524, 2016, doi: https://doi.org/10.1021/acsami.6b05538.
11. F. K. Shieh *et al.*, "Imparting Functionality to Biocatalysts via Embedding Enzymes into Nanoporous Materials by a de Novo Approach: Size-Selective Sheltering of Catalase in Metal-Organic Framework Microcrystals," *Journal of the American Chemical Society*, vol. 137, no. 13, pp. 4276–4279, 2015, doi: https://doi.org/10.1021/ja513058h.
12. P. Li *et al.*, "Nanosizing a Metal-Organic Framework Enzyme Carrier for Accelerating Nerve Agent Hydrolysis," *ACS Nano*, vol. 10, no. 10, pp. 9174–9182, 2016, doi: https://doi.org/10.1021/acsnano.6b04996.
13. T. N. A. Tuan Kob, M. F. Ismail, M. B. Abdul Rahman, K. E. Cordova, and M. A. Mohammad Latif, "Unraveling the Structural Dynamics of an Enzyme Encapsulated within a Metal–Organic Framework," *J. Phys. Chem. B*, vol. 124, no. 18, pp. 3678–3685, May 2020, doi: https://doi.org/10.1021/acs.jpcb.0c02145.
14. P. J. Patil, S. A. Kamble, M. J. Dhanavade, X. Liang, C. Zhang, and X. Li, "Molecular Modeling Insights into Metal-Organic Frameworks (MOFs) as a Potential Matrix for Immobilization of Lipase: An *In Silico* Study," *Biology*, vol. 12, no. 8, p. 1051, Jul. 2023, doi: https://doi.org/10.3390/biology12081051.
15. E. Karimian *et al.*, "The enzymatic synthesis of lactose caprate using *Candida rugosa* lipase immobilized into ZIF-8 and investigation of its anticancer applications against K562 leukemia and HeLa cancer cells," *RSC Adv.*, vol. 13, no. 50, pp. 35639–35647, 2023, doi: https://doi.org/10.1039/D3RA04632J.
16. J. Lin *et al.*, "Biomimetic Mineralization of Metal Ion-Doped Lipase into ZIF-8 Framework for Enhanced Hydrolytic Activity in Biphasic System," *ChemistrySelect*, vol. 7, no. 38, p. e202202721, Oct. 2022, doi: https://doi.org/10.1002/slct.202202721.
17. N. F. Hamidon, M. Ibrahim, M. Tahir, A. M. Latif, M. Basyaruddin, and A. Rahman, "Effect of altering linker ratio on nano-ZIF-8 polymorphisms in water-based and modulator-free synthesis," *Journal of Coordination Chemistry*, vol. 0, no. 0, pp. 1–13, 2022, doi: https://doi.org/10.1080/00958972.2022.2100990.
18. N. F. Hamidon, M. I. M. Tahir, M. A. M. Latif, and M. B. Abdul Rahman, "Influence of ZIF-8 polymorphism catalysts and nanosizes in *p*-nitrophenyl ester hydrolysis," *Applied Organom Chemis*, vol. 37, no. 7, p. e7136, Jul. 2023, doi: https://doi.org/10.1002/aoc.7136.
19. Y. Rodríguez-Mejía, N. K. R. Bogireddy, F. Romero-Romero, M. V. Basavanag-Unnamatla, V. Agarwal, and V. Varela-Guerrero, "*In situ* fabrication of ZIF-8 decorated tezontle for enzyme immobilization towards biodiesel production," *RSC Adv.*, vol. 15, no. 33, pp. 26632–26646, 2025, doi: https://doi.org/10.1039/D5RA02711J.
20. Y. Xiao, Y. Chen, R. Lu, Y. Wang, and C. Wang, "Immobilization of *Candida rugosa* lipase (CRL) on a hierarchical magnetic zeolitic imidazole framework-8 for efficient biocatalysis," *Biochemical Engineering Journal*, vol. 175, p. 108120, Nov. 2021, doi: https://doi.org/10.1016/j.bej.2021.108120.
21. L. Z. Cheong, Y. Wei, H. Wang, Z. Wang, X. Su, and C. Shen, "Facile fabrication of a stable and recyclable lipase@amine-functionalized ZIF-8 nanoparticles for esters hydrolysis and transesterification," *Journal of Nanoparticle Research*, vol. 19, no. 8, 2017, doi: https://doi.org/10.1007/s11051-017-3979-3.
22. M. Jian, B. Liu, R. Liu, J. Qu, H. Wang, and X. Zhang, "Water-based synthesis of zeolitic imidazolate framework-8 with high morphology level at room temperature," *RSC Adv.*, vol. 5, no. 60, pp. 48433–48441, 2015, doi: https://doi.org/10.1039/C5RA04033G.
23. Y. Pan, Y. Liu, G. Zeng, L. Zhao, and Z. Lai, "Rapid synthesis of zeolitic imidazolate framework-8 (ZIF-8) nanocrystals in an aqueous system.," *Chemical communications (Cambridge, England)*, vol. 47, no. 7, pp. 2071–3, 2011, doi: https://doi.org/10.1039/c0cc05002d.
24. D. N. Ta, H. K. D. Nguyen, B. X. Trinh, Q. T. N. Le, H. N. Ta, and H. T. Nguyen, "Preparation of Nano-ZIF-8 in Methanol with High Yield," vol. 96, no. January, pp. 1518–1531, 2018, doi: https://doi.org/10.1002/cjce.23155.
25. E. L. Bustamante, J. L. Fernández, and J. M. Zamaro, "Influence of the solvent in the synthesis of zeolitic imidazolate framework-8 (ZIF-8) nanocrystals at room temperature," *Journal of Colloid and Interface Science*, vol. 424, pp. 37–43, 2014, doi: https://doi.org/10.1016/j.jcis.2014.03.014.
26. B. Mohd. Abdul Rahman, U. H. Zaidan, M. Basri, Mohd. Z. Hussein, R. N. Z. R. Abd. Rahman, and A. B. Salleh, "Enzymatic synthesis of methyl adipate ester using lipase from *Candida rugosa* immobilised on Mg, Zn and Ni of layered double hydroxides (LDHs)," *Journal of Molecular Catalysis B: Enzymatic*, vol. 50, no. 1, pp. 33–39, Jan. 2008, doi: https://doi.org/10.1016/j.molcatb.2007.09.020.
27. M. M. Bradford, "A rapid and sensitive method for the quantitation of microgram quantities of protein utilizing the principle of protein-dye binding," *Analytical Biochemistry*, vol. 72, pp. 248–254, 1976.
28. F.-S. Liao *et al.*, "Shielding against Unfolding by Embedding Enzymes in Metal–Organic Frameworks via a *de Novo* Approach," *Journal of the American Chemical Society*, p. jacs.7b01794, 2017, doi: https://doi.org/10.1021/jacs.7b01794.
29. N. Saisuburamaniyan, L. Krithika, K. P. Dileena, S. Sivasubramanian, and R. Puvanakrishnan, "Lipase assay in soils by copper soap colorimetry," *Analytical Biochemistry*, vol. 330, no. 1, pp. 70–73, Jul. 2004, doi: https://doi.org/10.1016/j.ab.2004.04.016.
30. A. Zare, A.-K. Bordbar, F. Jafarian, and S. Tangestaninejad, "*Candida rugosa* lipase immobilization on various chemically

modified Chromium terephthalate MIL-101," *Journal of Molecular Liquids*, vol. 254, pp. 137–144, Mar. 2018, doi: https://doi.org/10.1016/j.molliq.2018.01.097.

31. C. S. Almeida, F. S. Neto, P. da S. Sousa, F. I. da S. Aires, J. R. de M. Filho, A. L. G. Cavalcante, P. G. Sousa Junior, R. L. F. Melo, and J. C. S. dos Santos, "Enhancing Lipase Immobilization via Physical Adsorption: Advancements in Stability, Reusability, and Industrial Applications for Sustainable Biotechnological Processes," *ACS Omega*, vol. 9, no. 47, pp. 46698–46732, Nov. 2024, https://doi.org/10.1021/acsomega.4c07088.
32. H. Zhang, H. Jiang, F. Yu, H. Zhang, Y. Wu, M. Shi, and C. Wang, "Advances in Lipase Immobilization and Applications in Biofabrication," *Reaction Chemistry & Engineering*, vol. 11, 2026, https://doi.org/10.1039/D5RE00493D.
33. C. E. Orrego, N. Salgado, J. S. Valencia, G. I. Giraldo, O. H. Giraldo, and C. A. Cardona, "Novel chitosan membranes as support for lipases immobilization: Characterization aspects," *Carbohydrate Polymers*, vol. 79, no. 1, pp. 9–16, Jan. 2010, doi: https://doi.org/10.1016/j.carbpol.2009.06.015.
34. K. Liang *et al.*, "Biomimetic mineralization of metal-organic frameworks as protective coatings for biomacromolecules," *Nat Commun*, vol. 6, no. 1, p. 7240, Jun. 2015, doi: https://doi.org/10.1038/ncomms8240.
35. D. Li *et al.*, "A facile one-pot synthesis of hemin/ZIF-8 composite as mimetic peroxidase," *Materials Letters*, vol. 178, pp. 48–51, Sep. 2016, doi: https://doi.org/10.1016/j.matlet.2016.04.200.
36. N. H. B. Yahya, Y. F. Yeong, and L. S. Lai, "Synthesis of Amino-Impregnated ZIF-8 for CO_2 Adsorption," *IOP Conf. Ser.: Mater. Sci. Eng.*, vol. 226, p. 012164, Aug. 2017, doi: https://doi.org/10.1088/1757-899X/226/1/012164.
37. W. Yang *et al.*, "Insights into the Interaction between Immobilized Biocatalysts and Metal–Organic Frameworks: A Case Study of PCN-333," *JACS Au*, vol. 1, no. 12, pp. 2172–2181, Dec. 2021, https://doi.org/10.1021/jacsau.1c00226.
38 L. Qi, Z. Luo, and X. Lu, "Biomimetic Mineralization Inducing Lipase–Metal–Organic Framework Nanocomposite for Pickering Interfacial Biocatalytic System," *ACS Sustainable Chem. Eng.*, vol. 7, no. 7, pp. 7127–7139, Apr. 2019, doi: https://doi.org/10.1021/acssuschemeng.9b00113.